Adaptable Ring for Vision-Based Measurements and Shape Analysis

Kanakam Teja Maddala, Randy H. Moss, *Senior Member, IEEE*, William V. Stoecker, Jason R. Hagerty, Justin G. Cole, Nabin K. Mishra, and R. Joe Stanley, *Senior Member, IEEE*

***Abstract*— A vision-based measurement approach for pill shape detection is presented along with other applications. Rapid and accurate pill identification is needed by medical and law enforcement personnel during emergencies. But real-world pill identification is challenging due to varied lighting conditions, minor manufacturing defects, and subsequent pill wear. Surmounting these challenges is possible using multiple inputs: pill color, imprint, and shape. Of these different inputs, pill shape is the most important and difficult parameter due to its variations. In this paper, we describe a novel technique to accurately detect the complex pharmaceutical pill shapes using measurements derived from a superimposed adaptable ring centered automatically on either the shape's centroid or its bounding box midpoint determined based on the measurements from two other rings, namely the inner ring and the outer ring. It is shown that the measurements from the overlays of the adaptable ring suffice to successfully classify the shapes of the pills currently in the Pillbox database (U.S. National Library of Medicine, 2014) with an accuracy of 98.7%. Our method demonstrated higher accuracy when compared with Hu-moments on the same data set. Using logistic regression techniques, Hu-moments provided an accuracy of 96.6%. Though developed for the domain of pharmaceutical pill shapes, we discuss how the measurements from the adaptable ring can also be used in other industrial applications to increase the level of accuracy with the help of this real-time less computationally complex method.**

***Index Terms*— Automatic optical inspection, image shape analysis, shape measurement, vision-based measurement (VBM).**

I. Introduction

CAMERAS are now widely available, which are portable, affordable, and suitable for platforms incorporating automatic methods to generate vision-based measurements (VBMs). Pill identification by automatic methods is of interest to consumers, the medical industry, and law enforcement agencies. Concerned parents want to be able to identify pills that they may encounter in their children's possession. Caregivers for the elderly or infirm often need to be able to identify pills. The pharmaceutical industry in recent years has developed new packaging applications and has interest in automatic pill verification. Emergency room personnel and law enforcement officials have long envisioned the need to identify pills rapidly and automatically. The total number of fatal adverse drug events reported to the U.S. Food and Drug Administration increased 2.7-fold between 1998 and 2005 [1]. The problem is compounded by increasing numbers of patients taking many prescriptions as well as increased numbers of adverse reactions from those prescriptions.

According to the Centers for Disease Control and Prevention, more than 76% of Americans aged over 60 used more than two prescription drugs and 37% used five or more [2]. The medication identification process during admission can be lengthy, and drug identification errors during hospital or emergency room admission can account for a majority of the potentially harmful medication mistakes during hospitalization [3]. Therefore, automatic identification of pills addresses a growing problem with life-threatening implications. Shape detection of pills is a challenging task due to their uneven and complex shapes. We developed a method to produce measurements from the overlay of a virtual adaptable ring on a pharmaceutical pill image to determine its shape. The same overlay information can also be used in other applications, for example, measuring the number of teeth of any given mechanical gear. Moreover, VBM systems are emerging in technologies that can be useful in many industrial applications, such as fabric quality control [4], rubber profile inspection [5], rail head defect detection for railroad tracks [6], and food calorie measurement from images [7]. These applications can all reduce human labor and increase productivity by decreasing both inspection time and human errors [8].

Large pill image databases such as the Pillbox database from the National Library of Medicine (NLM) [9] are now available, allowing rapid development and testing of pill identification algorithms. There are several pill shape classifiers developed for pill recognition systems but many fail to have a good shape accuracy. Lee *et al.* [10] reported an identification accuracy of approximately 74% for a pill identification system. Hartl *et al.* [11] used the Studiers tube ES framework for a mobile phone app that focuses on speed. Madsen *et al.* [12] focused on color recognition, obtaining up to 98% color accuracy but only approximately 65% shape accuracy. Since multiple classifiers, both traditional and new classifiers, fail on pill shape classification, this adaptable-ring method was specifically designed for pill shapes, but can be customized

Manuscript received September 9, 2015; revised November 12, 2015; accepted December 14, 2015. Date of publication February 7, 2017; date of current version March 8, 2017. The Associate Editor coordinating the review process was Dr. Shervin Shirmohammadi.

K. T. Maddala, R. H. Moss, and R. J. Stanley are with the Department of Electrical and Computer Engineering, Missouri University of Science and Technology, Rolla, MO 65409-0040 USA (e-mail: kmhx9@mst.edu; rhm@mst.edu; stanleyj@mst.edu).

W. V. Stoecker, J. R. Hagerty, J. G. Cole, and N. K. Mishra are with Stoecker & Associates, Rolla, MO 65401 USA (e-mail: wvs@mst.edu; jrh55c@mst.edu; jgcpp9@mst.edu; nkmhd3@mst.edu).

Color versions of one or more of the figures in this paper are available online at http://ieeexplore.ieee.org.

Digital Object Identifier 10.1109/TIM.2017.2650738

for similar applications by evaluating the generated overlay measurements.

This paper presents a novel method for vision-based shape classification and compares the new method with Hu Moments in classifying pill shapes on the entire Pillbox database of the NLM. The order of the remaining sections of this paper is as follows: Section II gives a brief background on shape analysis; Section III describes the methodology, including pill detection, rotation, outer, inner, and adaptable ring determination, feature measurement, and classifier development; Section IV provides the results for both Hu Moments and the adaptable-ring algorithm, along with error analysis, and Section V discusses the results and uncertainties in measurement. Finally, Section VI provides a conclusion.

II. Background

General shape recognition algorithms for VBM are of two types: those that depend upon recognition of key points or landmarks, and those that do not rely on key points, but rather view the object outline as a continuous curve [13]. These two classes of algorithms have been termed, respectively, salient point algorithms and gestalt algorithms, with the older literature emphasizing detection of key or salient points [14], some studies emphasizing global or gestalt features [13], [15], and still other authors detecting both types of features. Geometric shapes such as polygons have been studied extensively.

A chain code algorithm developed by Freeman [13] can detect regular polygons by representing their boundaries and corner points where direction is changed from one chain to another. Another shape detector for regular polygons was developed by Barnes *et al.* [16]. The algorithm used an approximation of a maximum likelihood image, which is convolved with a weighted angular histogram. This was used to detect road signs successfully in natural images [17]. This approach is not optimal for pill shapes due to the rounded pill corners.

However, for a VBM system to detect the irregular shapes, we need to get quantifiable measurements from the image, as reported here using an adaptable-ring technique. A somewhat similar system by Pouladzadeh *et al.* [7] measures the area of food portion on a plate by superimposing a grid of squares each with equal area. Another system by Nandi *et al.* [18] for mango ripeness measurement uses chain codes to trace the fruit boundary, which is then rotated vertically by finding its maximum axial length. Gan and Zhao [19] used an active contour model to identify visual defects in an LCD panel. This method highlights the irregularly shaped defect but in order to further classify the defect or anomaly into specific categories, measurements from that irregular anomaly on the panel are needed.

One of the most popular shape classification techniques is the invariant moments technique proposed by Hu [20]. This method is widely used for image shape recognition in a variety of applications due to its invariance to object translation, scaling, and rotation. It is assumed that images are relatively free of noise. Most pill identification applications published to date use Hu Moments to describe the pill shape [10], [12]; however, thorough details are lacking in these reports. Therefore, it is desirable to compare new methods that are developed for real-time use, and to report details of the database, detection methods, and detection accuracy.

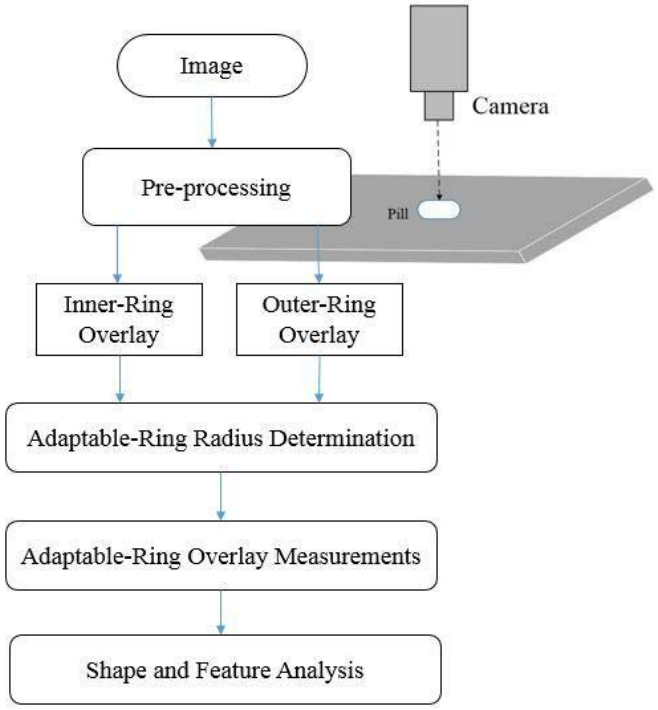

Fig. 1. Workflow for pill shape detection.

III. Methodolgy and Approach

A. Image Database and Overall Workflow

There were 2151 high resolution pill images in the Pillbox database as of December 2014 [9]. These pill images were taken with a visible light camera mounted perpendicularly over the pill and are of very high quality and resolution with controlled illumination and uniform background. These merits of the database allow segmentation by simple threshold to separate the pill object from the background for almost all pills. More images were added to Pillbox later, many of which are of lower quality. But for a real-time system, we recommend that the camera be mounted perpendicularly and the object be placed on a black background to avoid shadows and that even illumination be provided. After preprocessing, an inner ring and an outer ring are superimposed on the segmented pill. Then the radius for the adaptable ring is determined, followed by its overlay measurements to classify the pill shape. The workflow diagram is shown in Fig. 1.

B. Preprocessing

The uniform background pixels in the image were replaced with black pixels. Next, imprints on 1% of the pills caused holes in the segmented objects, which were found and filled automatically after thresholding to obtain very accurate pill shapes. All pixels that exceed an optimized gray-level threshold and area filtering are classified as pill. Two pill objects, pill

TABLE I
LIST OF AVAILABLE SHAPES IN PILLBOX WEBSITE [9]

Available pill shapes defined by pillbox	
Capsule	Square
Diamond	Pentagon
Oval	Hexagon
Trapezoid	Hexagon (shield)
Tear	Triangle
Rectangle	Round
Octagon	Freeform

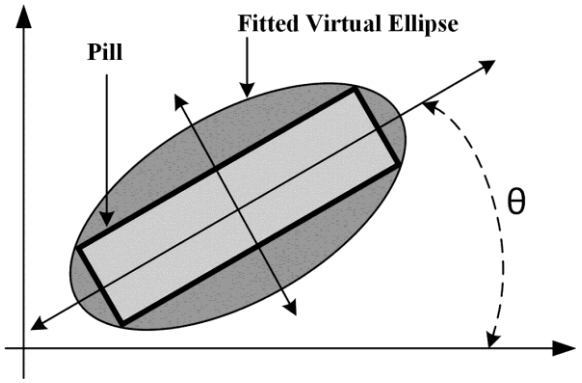

Fig. 2. Orientation of pill.

obverse and reverse, are now present in the processed Pillbox images. The first object encountered in left-to-right then top-to-bottom search is selected as the pill shape. This shape and the surrounding bounding box resolution were increased by padding with black pixels to allow construction of the surrounding rings in later steps. The resulting binary image contains just pill (white pixels) and padded background (black pixels). The 14 shapes defined by Pillbox are shown in Table I.

C. Rotation of the Pill

To make the process rotation-invariant, the angle (θ) between the orientation of the major axis of the ellipse fit around the pill and the horizontal axis is determined by the "*orientation"* property of MATLAB's "*regionprops"* function, as shown in Fig. 2. The pill shape is then rotated in the clockwise direction with the same angle (θ), to make the pill's longest axis horizontal.

D. Outer- and Inner-Rings

The rotated pill image is now oriented with the longest axis in the horizontal direction. Then the pill bounding box is determined prior to superimposition of the rings. The diameter of the outer ring is defined as the length of the pill bounding box in the horizontal direction. This diameter is therefore the least diameter to intersect the outer edge of a given shape in the horizontal direction**.** The diameter of the inner ring is the maximum height of the bounding box perpendicular to the horizontal axis. The width of both the rings can be customized

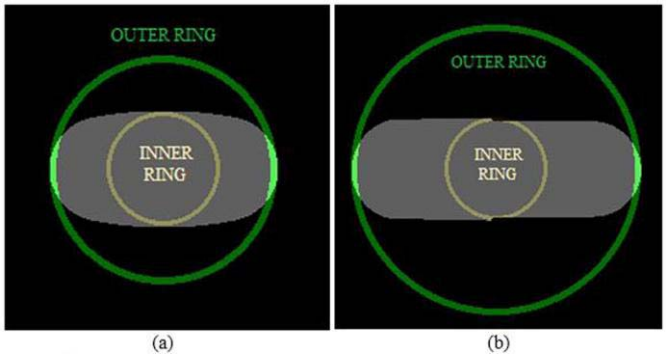

Fig. 3. (a) Oval pill with outer and inner ring overlays. (b) Capsule with outer and inner ring overlays. The inner ring has asymmetric right-to-left overlays at the midpoint due to different capsule widths at the capsule seam.

depending on the height of the camera, the resolution of the segmented image and the application involved. In this case, the inner ring is three pixels wide and the outer-ring is five pixels wide. Fig. 3(a) shows outer and inner rings and their overlays on an oval Pillbox pill. The overlays are the intersections of the inner ring and outer ring with the segmented pill. The inner ring overlays in Fig. 3(b) are different for the right and left capsule parts, allowing differentiation from an oval shape, with right–left symmetry. The areas of the right and left outer-ring and inner-ring overlays are saved. Then, the intersection of these rings is checked by identifying the unique color pixels created by overlapping of two different colored rings. This intersection check will give input arguments to determine the radius of the main ring, which will be called the adaptable ring. This overall process is shown in Fig. 4. Together with the pill area, the overlay measurements from this adaptable ring will provide decision tree arguments to discriminate pill shapes.

E. Determination of Adaptable Ring and Its Measurements

For a minority of shapes, the bounding box center will not suffice as the center of the adaptable ring. For the triangle and pentagon shapes, the inner and outer rings as defined previously intersect wholly or partially as shown in Fig. 5(b). Whenever this intersection occurs, the adaptable-ring center is adjusted to lie at the pill centroid, so that the adaptable ring just touches the corners of the pill, as shown in Fig 5(c). Thus inner-ring and outer-ring intersection serves as a criterion for changing the adaptable-ring center from the bounding box center to the pill centroid. If this adjustment is not made, then measurements from the overlays caused by the adaptable ring may not be unique and useful for a triangular pill as shown in Fig. 6. Adjusting the center automatically when the criterion of intersecting inner and outer rings is matched, desired overlays are produced for the triangular pill as shown in Fig. 7. Using a lower gray level for the segmented pill and the adaptable ring will provide a higher gray level for overlays, which makes it easier to segment them in order to obtain measurements as shown in Figs. 5(d) and 7(b). For shapes with more than one axis of symmetry, such as circles, squares, and hexagons, the criterion is met, but this adjustment does not change anything,

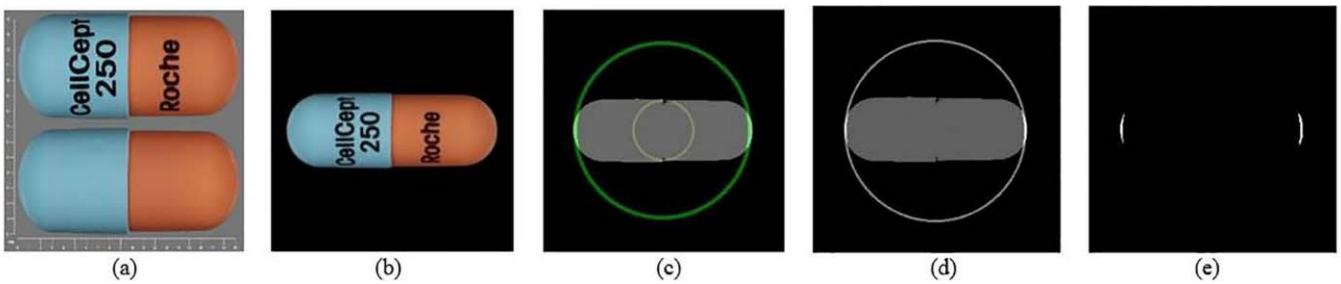

Fig. 4. Process—(a) Pillbox image, (b) extracted pill, (c) with inner and outer rings, (d) with super-imposed adaptable ring, and (e) overlays caused by adaptable ring.

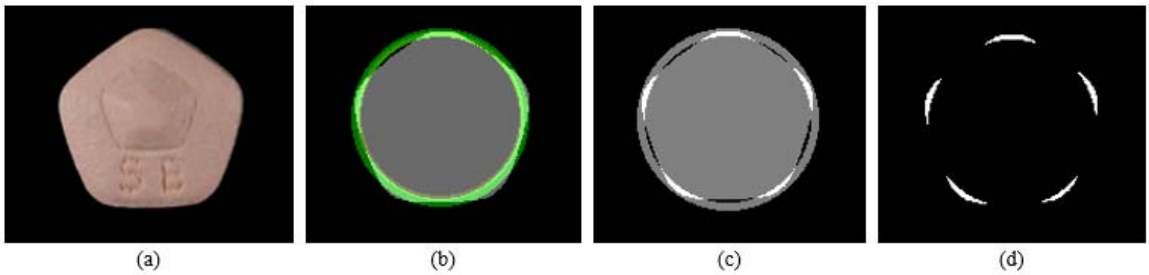

Fig. 5. Process—(a) Pentagon shaped pill, (b) with inner and outer rings intersected, (c) with adaptable ring, and (d) overlays caused by adaptable ring.

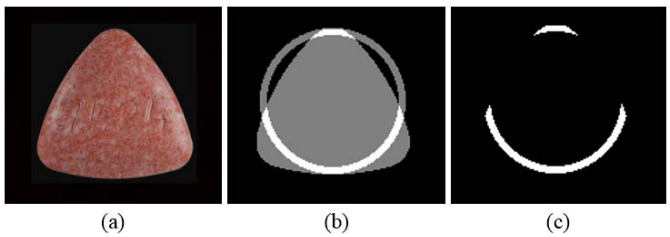

Fig. 6. Nonideal case—(a) Triangular pill. (b) Adaptable ring centered at bounding box center of the segmented pill and radius as given in (2). (c) Information from the overlays that may not be useful for classification.

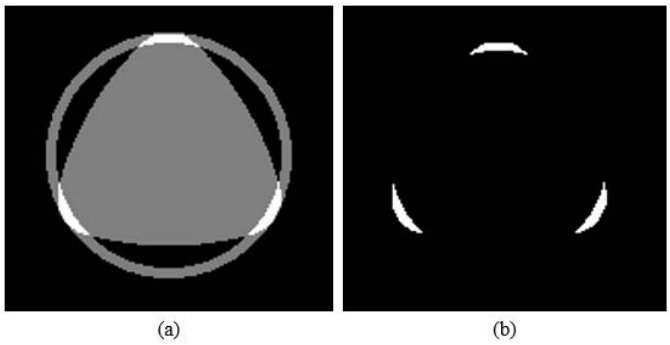

Fig. 7. Ideal case—(a) Adaptable ring centered at centroid of the triangular pill and radius as in (1). (b) Useful overlays caused by the adaptable ring, with width of the adaptable ring slightly increased for illustration purposes.

because the centroid of the shape and the center of the outer ring at the bounding box center are identical for these shapes. The width of the adaptable ring can be varied but only a single width should be used for the entire database in order to discriminate shapes based on the decision tree formed from the thresholds of overlay measurements.

The next step is to determine the radius of the adaptable ring. For shapes like round, square, and triangle, the inner-ring and outer-ring intersection criterion is met, and the adaptable ring is inscribed about the centroid of the pill with a radius of the longest distance from the center to the outer boundary of the pill. If $(Xc,\ Yc)$is the centroid of the pill and $(X,\ Y)$ are the coordinates of all points within the pill shape, then the adaptable-ring outer radius R is given as

$$R_{\text{adaptable-ring}} = \max\left[\sqrt{(Xc - X)^2 + (Yc - Y)^2}\right]. \quad (1)$$

In the next case, when an oval, capsule, rectangle or trapezoidal pill is considered, the inner-ring and outer-ring intersection criterion is not met. The center of the ring in this case will be the center of the bounding box of the pill rather than the centroid. The length of the major-axis of the pill is determined by the length of longest side of the pill bounding box, therefore the outer radius of the adaptable ring is half the length of the pill major axis as given as

$$R_{\text{adaptable-ring}} = \frac{(\text{LengthofMajorAxisofPill})}{2}. \quad (2)$$

The adaptable-ring radius determination proceeds as mentioned previously for each pill. The primary measurement provided by the adaptable ring is the number of overlays, which alone can classify most of the pill shapes. The remaining shapes will use other measurements such as the area of overlays of both adaptable ring and inner ring along with the shape area and its bounding box area. The overall process along with the adaptable ring is shown in Figs. 4 and 5.

F. Shape Classification From the Overlay Measurements

Fig. 8 shows how several pill shapes are classified according to the number of overlays; here, it refers to the count of

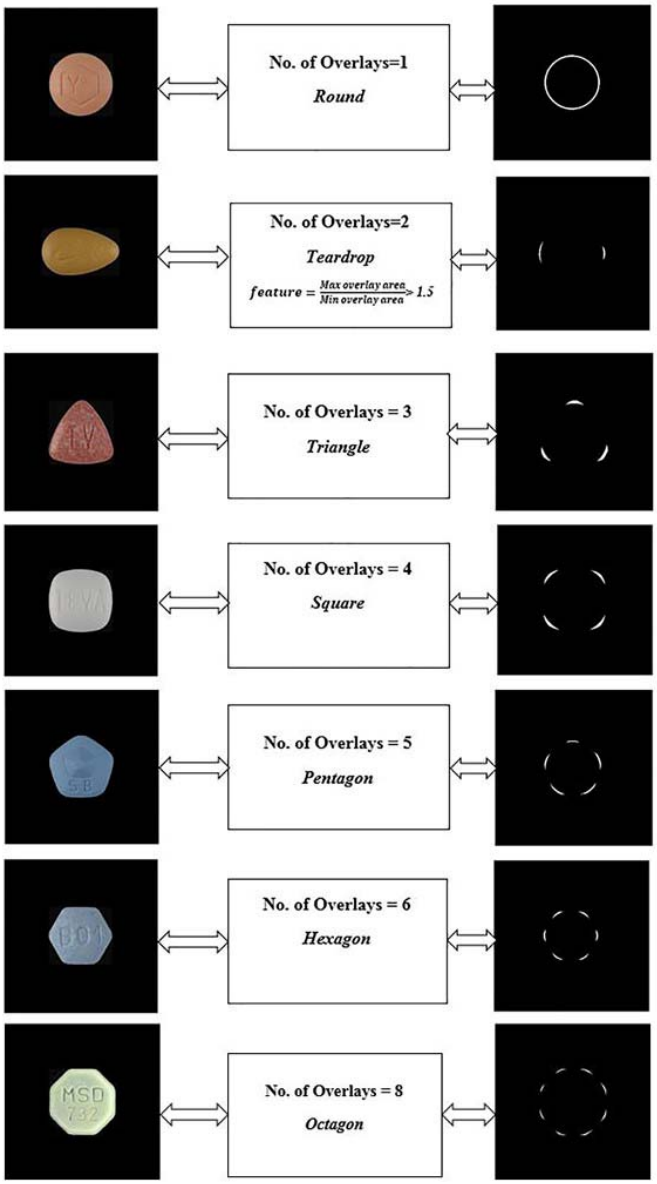

Fig. 8. Segmented pill shape classification using overlays of adaptable ring on pill.

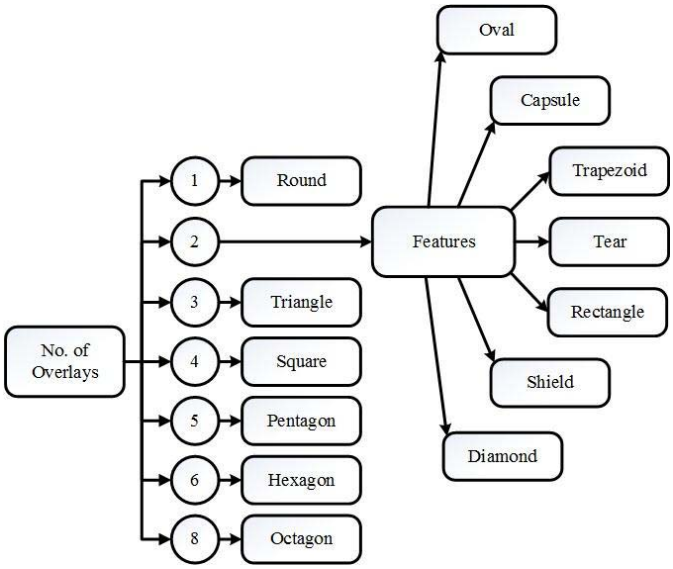

Fig. 9. Classification of pill shapes with adaptable-ring overlays. If a given pill does not meet the criteria for any of the shapes shown, it is classified as freeform.

TABLE II
FEATURES USED TO DETECT AND CLASSIFY PILL SHAPE

Feature No.	Description
1	Number of adaptable-ring overlays
2	$\frac{\text{Max adaptable ring overlay area}}{\text{Min adaptable ring overlay area}}$
3	$\frac{\text{Inner ring overlay Area}}{\text{Total inner ring Area}}$
4	$\frac{\text{Area of pill}}{\text{Area of pill bounding box}}$
5	$\frac{\text{Area of right half of inner ring overlay}}{\text{Area of left half of inner ring overlay}}$
6	$\frac{\text{Max adaptable ring overlay area}}{\text{Area of pill}}$

adaptable-ring overlays on the pill shape. For example, if there are three overlays, then the pill is triangular. These overlay numbers suffice to classify many shapes including round, triangle, square, pentagon, hexagon, and octagon shapes to form a decision tree. Only when two overlays occur are more features required (Fig. 9).

Various features are defined from the overlay measurements in the algorithm to detect the proper pill shape when there are two overlays. The number of features and their criteria can be varied according to the objects to be classified. For classifying shapes in the Pillbox database, we have defined six size-invariant features, and these are presented in Table II. Moreover, the criteria of features to determine a particular shape using these features are shown in Table III. These empirical values for each feature criterion for each shape are obtained from observing samples of each shape. These samples amounted to fewer than 100 images of all shapes together. These criteria for features were checked sequentially to complete the decision tree for the case when there were two overlays. If any new geometrical shapes are added to the database, the algorithm can be modified easily by defining features and obtaining empirical values as thresholds in such a way to identify the shape of the desired object.

The features used in Table II were also used to train a neural network with disjoint training, validation, and test sets of images. For the neural network, six input neurons, ten hidden neurons, and 14 output neurons were used. Section IV shows the results and a comparison with the Hu moments method.

TABLE III
FEATURE CRITERIA WHEN TWO OVERLAYS OCCUR

Shape	Feature Criterion
Shield	Feat2>4
Diamond	Feat3<1.2 & Feat2<1.2 & Feat4<0.75
Trapezoid	Feat2>0.9 & Feat6<0.009
Teardrop	Feat2>1.5 & Feat4<0.81
Rectangle	Feat2<1.3 & Feat3>0.90 & Feat4>0.94
Oval	Feat2<1.1 & Feat3>0.99 & $\lvert$Feat5-1$\rvert$<0.01
Capsule	1<Feat2<1.5 & Feat3>0.8 & $\lvert$Feat5-1$\rvert$>0.01

TABLE IV
PERFORMANCE OF NEURAL NETWORK ON 1652-IMAGE TEST SET

Shape	Total Test Images	Detected	Detection Rate (%)
Round	979	977	99.8
Triangle	5	5	100
Square	4	4	100
Pentagon	4	4	100
Hexagon	2	2	100
Octagon	1	1	100
Oval	490	471	96.1
Capsule	149	132	88.5
Trapezoid	1	1	100
Tear	5	5	100
Rectangle	2	1	50
Shield	3	3	100
Diamond	4	4	100
Freeform	3	0	0

IV. RESULTS

A. Identification of Shapes of Pillbox Pills

The adaptable-ring algorithm works well on the Pillbox images. The existing Pillbox data set consists of 14 different shapes. These mostly high-quality images allow exact segmentation by thresholding. The overlay number produced by the adaptable ring is reliable in determining pill shape. For a round shape, the number of overlays of the adaptable ring on the pill surface is one. For a triangle-shaped pill, the number of overlays is three. Similarly, square, pentagon, hexagon, and octagon shapes yield four, five, six, and eight overlays, respectively. Thus, for all overlay numbers except two, the shape is determined entirely by the number of overlays as shown in Fig. 9. When there are two overlays, the feature criteria in Table III are needed to determine pill shape. As an example, in distinguishing a teardrop shape from an oval shape, features 2 and 4 are employed (Table III). The same database of Pillbox images was also used to generate results with Hu moments.

B. Results of Adaptable-Ring Algorithm With Neural Network

A neural network was used to classify inputs from Table II into a set of target categories (14 shape classes in this case). The input layer consists of six neurons and the output layer consists of 14 neurons for 14 shape classes. The data set is divided into a 400-image training set, a 100-image validation set, and a 1652-image testing set. The training images consist of 50 round pills, 69 capsules, 250 oval pills, and the remaining 31 pills are comprised of all the remaining shapes. Note that one non-Pillbox image of an octagon pill is added to the testing set as there is only one octagon pill in the previous 2151 image data set. So the entire data set used for the neural network consists of 2152 images. A small number of images for certain shapes makes it difficult to separate training and testing sets, which is a limitation of the available data set. The validation set consists entirely of round, capsule, and oval shapes. The network is trained with a scaled conjugate gradient backpropagation algorithm, and the results obtained on the test set are shown in Table IV, which shows the total number of test images for each shape and the number that were correctly classified along with the detection rate. Overall, 97.5% of the 1652 pills in the test set were classified correctly. The results obtained with the neural network clearly indicate that shapes depending on only overlay numbers have a higher detection rate for this data set.

C. Results with Hu Moments

Hu's invariant moments [20], [21], seven parameters obtained from shapes, are widely used in object shape detection and classification. However, when used for pill shape detection, these moments do not incorporate enough features to distinguish some shapes. The difficult pill shapes (with the number misclassified) are oval (23), capsule (12), and pentagon (8), which together comprise 43 (59%) of the total 73 misclassified pill shapes. In 23 of the total 73 misclassified examples, the shape is not classified as geometric, but rather freeform: i.e., not enough information is available to classify the pill. Moreover, all the pentagons (8), hexagons (3), shields (5), and octagon (1) are misclassified as round. The overall accuracy for the Hu Moments method is 96.61%. The confusion matrix for Hu Moments, which displays predicted results (columns) versus actual results (rows), is shown in Table V. (For example, 231 capsules were correctly classified, while seven capsules were incorrectly classified as ovals and five as freeform.) From this matrix, it can be clearly seen how the Hu moments were unable to detect the squares, hexagons, shields, octagon, and pentagons, which were mostly misclassified as round.

In order to recognize the round-shaped pills by Hu's seven invariants it was enough to use the first invariant I_1 to get separation from the rest of the shapes. Moreover, there

TABLE V
CONFUSION MATRIX FOR HU MOMENTS METHOD APPLIED ON 2151-IMAGE DATA SET

Actual Shape \ Predicted Shape	Capsule	Diamond	Hexagon	Oval	Pentagon	Rectangle	Round	Square	Tear	Trapezoid	Triangle	Shield	Octagon	Freeform	Total	FN	FN%
Capsule	**231**	0	0	7	0	0	0	0	0	0	0	0	0	5	*243*	*12*	*4.9%*
Diamond	0	**4**	0	4	0	0	0	0	0	0	0	0	0	0	*8*	*4*	*50%*
Hexagon	0	0	**0**	0	0	0	3	0	0	0	0	0	0	0	*3*	*3*	*100%*
Oval	2	0	0	**767**	0	0	4	0	0	0	0	0	0	17	*790*	*23*	*2.9%*
Pentagon	0	0	0	0	**0**	0	8	0	0	0	0	0	0	0	*8*	*8*	*100%*
Rectangle	0	0	0	3	0	**1**	0	0	0	0	0	0	0	0	*4*	*3*	*75%*
Round	0	1	0	2	0	0	**1050**	0	0	0	0	0	1	0	*1054*	*4*	*0.4%*
Square	0	1	0	1	0	0	5	**0**	0	0	0	0	0	0	*7*	*7*	*100%*
Tear	0	0	0	0	0	0	0	0	**9**	0	0	0	0	0	*9*	*0*	*0%*
Trapezoid	0	0	0	0	0	0	0	0	0	**2**	1	0	0	0	*3*	*1*	*33.3%*
Triangle	0	0	0	0	0	0	1	0	0	0	**8**	0	0	1	*10*	*2*	*20%*
Shield	0	0	0	0	0	0	5	0	0	0	0	**0**	0	0	*5*	*5*	*100%*
Octagon	0	0	0	0	0	0	1	0	0	0	0	0	**0**	0	*1*	*1*	*100%*
Freeform	0	0	0	0	0	0	0	0	0	0	0	0	0	**6**	*6*	*0*	*0%*
TP+FP	*233*	*6*	*0*	*784*	*0*	*1*	*1077*	*0*	*9*	*2*	*9*	*0*	*1*	*29*			
FP	*2*	*2*	*0*	*17*	*0*	*0*	*27*	*0*	*0*	*0*	*1*	*0*	*1*	*23*			
FP%	*0.9%*	*33.3%*	*0%*	*2.2%*	*0%*	*0%*	*2.5%*	*0%*	*0%*	*0%*	*11.1%*	*0%*	*100%*	*79.3%*			

were eight pentagon-shaped pills, where all eight pills were misclassified as round-shaped pills by Hu moments. In contrast, the adaptable-ring algorithm detected all eight of them correctly as pentagons. Shapes for which 100% Hu moments misclassification occurred are round-cornered shapes, such as square, pentagon, shield, hexagon, and octagon, and the most frequent erroneous shape chosen is round. Logistic regression shows that the most accurate classification for nearly all the shapes above-mentioned, except for the oval shape, is done with I_1 alone. For the oval shape, I_1–I_7 are all needed. Analysis by logistic regression (SAS Proc Logit) shows no additional classification benefit for these higher moments. Linear regression also shows correct classification for 1050 of the 1054 round pills using only the first moment I_1, reliability which leads to a choice of I_1 alone for classification. Therefore, by logistic regression analysis, these shapes cannot be reliably separated using these seven Hu moments.

D. Results of Adaptable-Ring Algorithm With Decision Tree

A total of 98.7% of pill shapes in the data set are identified correctly by the adaptable-ring algorithm using the empirical values as defined in the decision tree. The confusion matrix for this classification is shown in Table VI. Rows represent actual shape and columns represent predicted shape. TP denotes the true positives, and FP and FN denote the false positives and the false negatives, respectively. This data set consists mostly of these common shapes: round (1054), oval (790), and capsule (243), for a total of 2087 (97%) of the 2151 shapes. The errors in the algorithm are mostly in these three shapes: round (3), oval (11), and capsule (13). Only one other error is found: an error in the freeform shape, making a total of 28 errors as opposed to 73 in the case of Hu moments. As opposed to the neural network classifier, the decision tree classifier uses fewer than 100 shape samples to obtain the empirical values in Table III and classifies the entire data set of 2151 images.

E. Examples of Shape Mismatches

The primary data set consists of mostly round pills, oval pills, and capsules. There are a total of 1054 round pills, out of which 1051 pills were detected as round. The remaining three pills, which have rough broken edges, were detected as freeform-shaped pills by the algorithm. "Freeform" in this classification is defined as any shape that does not meet the shape criteria for the other 13 defined shapes. Note that "freeform" is also one of the 14 defined Pillbox shapes and that in Pillbox there exist only six highly variable pills, for which examples include double-circle, heart-shape, inverted arc, and T-shaped pills for which the number of overlays is three for only the heart-shaped pill, leading to its misclassification. In Section V, performance evaluation and uncertainties will be discussed along with other potential industrial applications.

V. DISCUSSION AND EVALUATION

Detecting pill shapes is a challenging task due to their smooth, round corners as opposed to the sharp corners present in ideal polygons. The adaptable-ring algorithm mainly uses the overlays and other unique features of the inner and the adaptable ring. Overall, the decision tree classification based on just overlay numbers was done 1080 times, and the linear classifier based on Table III was invoked 1071 times for the 2151 image data set. For the oval class, error was caused by the linear classifier eight out of 13 times, and for the capsule class, eight out of 11 times. This novel technique can yield a high classification rate for the regular and rounded shapes characteristic of pills. Several pill image retrieval techniques were developed by others over the past five years [10], [11], [22], [23], and [24]. In these techniques, the emphasis was in retrieving the pill from the database, but the performance in detecting its shape during the retrieval process is not always fully documented.

TABLE VI
CONFUSION MATRIX FOR ADAPTABLE-RING METHOD WITH DECISION TREE CLASSIFICATION APPLIED ON 2151-IMAGE DATA SET

Actual Shape \ Predicted Shape	Capsule	Diamond	Hexagon	Oval	Pentagon	Rectangle	Round	Square	Tear	Trapezoid	Triangle	Shield	Octagon	Freeform	Total	FN	FN%
Capsule	**230**	0	0	6	0	0	0	0	0	2	4	0	0	1	*243*	*13*	*5.3%*
Diamond	0	**8**	0	0	0	0	0	0	0	0	0	0	0	0	*8*	*0*	*0%*
Hexagon	0	0	**3**	0	0	0	0	0	0	0	0	0	0	0	*3*	*0*	*0%*
Oval	3	5	0	**779**	0	0	0	0	0	0	0	0	0	3	*790*	*11*	*1.4%*
Pentagon	0	0	0	0	**8**	0	0	0	0	0	0	0	0	0	*8*	*0*	*0%*
Rectangle	0	0	0	0	0	**4**	0	0	0	0	0	0	0	0	*4*	*0*	*0%*
Round	0	0	0	0	0	0	**1051**	0	0	0	0	0	0	3	*1054*	*3*	*0.3%*
Square	0	0	0	0	0	0	0	**7**	0	0	0	0	0	0	*7*	*0*	*0%*
Tear	0	0	0	0	0	0	0	0	**9**	0	0	0	0	0	*9*	*0*	*0%*
Trapezoid	0	0	0	0	0	0	0	0	0	**3**	0	0	0	0	*3*	*0*	*0%*
Triangle	0	0	0	0	0	0	0	0	0	0	**10**	0	0	0	*10*	*0*	*0%*
Shield	0	0	0	0	0	0	0	0	0	0	0	**5**	0	0	*5*	*0*	*0%*
Octagon	0	0	0	0	0	0	0	0	0	0	0	0	**1**	0	*1*	*0*	*0%*
Freeform	0	0	0	0	0	0	0	0	0	0	1	0	0	**5**	*6*	*1*	*16.7%*
TP+FP	*233*	*13*	*3*	*785*	*8*	*4*	*1051*	*7*	*9*	*5*	*15*	*5*	*1*	*12*			
FP	*3*	*5*	*0*	*6*	*0*	*0*	*0*	*0*	*0*	*2*	*5*	*0*	*0*	*7*			
FP%	*1.3%*	*38.5%*	*0%*	*0.8%*	*0%*	*0%*	*0%*	*0%*	*0%*	*40%*	*33.3 %*	*0%*	*0%*	*58.3%*			

TABLE VII
EVALUATION OF TWO IRREGULAR SHAPES WITH DIFFERENT METHODS. OUR METHOD USES DECISION TREE CLASSIFICATION

Irregular Shapes	Methods	Total pills of that shape	FN	FP	Pr (%)	Rc (%)
Capsule	*Hu Moments*	243	12	2	99.14	95.06
	Our Method		13	3	98.71	94.65
Oval	*Hu Moments*	790	23	17	97.83	97.09
	Our Method		11	6	99.24	98.61

A. Comparison With Hu Moments

To compare the performance of the proposed algorithm with Hu moments, *Sensitivity* as in (3) and *Specificity* as in (4) are used. Detection rate (5), defined the same as *Sensitivity,* is used to assess the accuracy. Here, TN denotes the true negatives, and TP, FP, and FN are as defined earlier

$$\text{Sensitivity or Recall}(R_c) = \frac{\sum \text{TP}}{(\sum \text{TP} + \sum \text{FN})} \times 100\% \quad (3)$$

$$\text{Specificity} = \frac{\sum \text{TN}}{(\sum \text{FP} + \sum \text{TN})} \times 100\% \quad (4)$$

$$\text{Detection Accuracy} = \frac{\sum \text{TP}}{(\sum \text{TP} + \sum \text{FN})} \times 100\% \quad (5)$$

$$\text{Precision}(Pr) = \frac{\sum \text{TP}}{(\sum \text{TP} + \sum \text{FP})} \times 100\%. \quad (6)$$

TN, TP, FN, and FP are determined from the confusion matrices for Hu Moments and adaptable-ring as shown in Tables V and VI, respectively. As rows represent the actual shape and columns represent the predicted shape for each shape category, it is easier to determine total FN for each shape by summing the misclassifications across its row, and similarily to determine total FP for each shape by summing the misclassifications across its column.

The adaptable-ring method achieves a detection accuracy of 98.7% and an error rate of 1.3% as compared with the error rate of 3.4% for Hu Moments. This technique is more accurate than Hu moments primarily because errors are reduced in the common shapes, such as square, pentagon, triangle, hexagon, and oval for a total of 28 errors instead of 73 in the case of Hu moment invariants. Detection accuracy of Hu moment invariants was 96.61% on a data set of 2151 images. The neural network's detection accuracy was 97.5%, but we must note the limited availability of certain shapes in its test set.

Two of the most misclassified shapes in the data set are capsule and oval. We used Precision (Pr) and Recall (Rc) as comparison criteria as they are widely used by the pattern recognition and information retrieval communities [25]. Table VII represents the comparison for these two shapes in terms of precision and recall as defined in (6) and (3), respectively. For capsules, Hu moments has a slightly higher precision but it is clear that the adaptable-ring method has a better performance with the large number of irregular ovals.

Cunha *et al.* [22] used Hu invariant moments in their mobile application named *helpmepills* to detect pills. Shape detection in this application uses Hu moments after segmenting the pill, which is placed on a black background followed by Hu moments comparison from an ideal set of images. However,

TABLE VIII
TIME TAKEN TO DETECT SHAPE FROM AN IMAGE WITH THE ADAPTABLE-RING METHOD USING THE DECISION TREE CLASSIFIER

	Mean	Standard deviation
Elapsed Time (seconds)	0.53	0.16

their algorithm was designed to detect only eight pill shapes and does not separate capsule from oval because it defines both shapes under a single class called oblong. Shape accuracy was not documented.

B. Other Applications

The adaptable-ring method can be combined with any simple VBM system to analyze shapes. As an example, we can automatically count the number of teeth of mechanical gears by measuring the adaptable-ring overlays on gears or any similar object, as a check for manufacturing defects. This approach provides a fast and accurate way to count the gear teeth. Fig. 10 shows how the adaptable-ring overlay aided in calculating the number of gear teeth.

C. Limitations and Measurement Uncertainty

This method describes an approach that overcomes a challenge in shape detection, where different shape variations exist within the same shape category, as in the oval class. We used the Pillbox images because it was the largest publicly available data set of pill images found. The images in this data set had a background of constant color, which simplified segmentation. In a real-world environment, a homogenous background would be ideal but we acknowledge that may not always be possible, and a solution to the segmentation problem is beyond the scope of this paper. Using different backgrounds for the image other than black would require a more complex segmentation technique, as there exist many multicolored medical pills. So, a black background is suggested for any pill identification system at least until a large database of pills on other backgrounds becomes available for research.

Uncertainties are inevitable for any vision-based system. Certain parameters need to be controlled, such as lighting to avoid uneven illumination. Uneven lighting impedes the process during preprocessing as shown in Fig. 11, where the right-most tooth is unevenly illuminated, and its effect can be seen in the reduced area of the ring's overlay in the output image.

Another uncertainty to take into account is the camera angle. Any change in the angle affects this method because the annularity of the object changes, which in turn will change the desired overlays. Any vibrations when the image is taken can also lead to false results. In order to get desired results with this system, the camera should be mounted perpendicularly with accurate focus along with even illumination with a black background preferred to avoid shadowing and to facilitate smoother preprocessing.

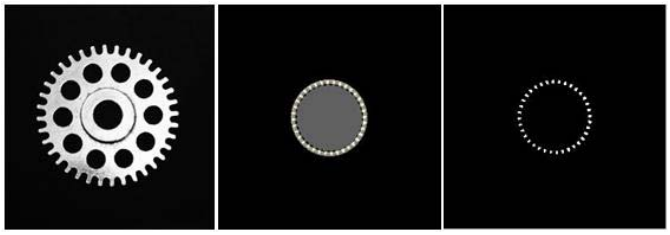

Fig. 10. Counting gear's teeth by measuring adaptable-ring overlays.

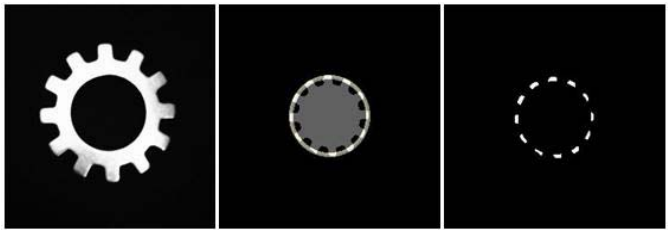

Fig. 11. Counting unevenly illuminated gear teeth.

There are also certain disadvantages and limitations to this system. There were limited numbers of certain shapes available in the data set. Hence performance on these shapes may be worse than performance on other shapes in a larger database. Most of the available data sets (other than Pillbox) are of low quality images and are also comprised mostly of ovals, rounds, and capsules.

Image noise also has the potential to cause problems with the proposed system. Image uncertainties can, in principle cause the number of ring overlays to vary. The ring widths were chosen to allow some robustness with respect to noise. It would take a significant amount of noise to break an overlay into two parts with the current ring widths, but ring width is a variable that could be adjusted to help compensate for image noise.

If multiple pills appear in the same image, then the shapes can be identified if the individual pills are accurately segmented and if the pills are not touching or overlapping.

D. Evaluation of Computational Complexity

Since this method is designed for real-time applications, we are considering the elapsed time as the primary factor in the evaluation of computational complexity. Also, with progress in computer technology, the memory factor is subsiding as both availability and affordability have increased. Hence, we calculated the elapsed time to detect a shape from the image by the adaptable-ring method. The program was implemented with MATLAB in a laptop with an Intel Core i7 CPU (2.6 GHz) and 8-GB RAM. The program was run on 2151 Pillbox images, and the mean and the standard deviation of the run time per image were calculated, respectively, as 0.53 $\pm$0.16 s, shown in Table VIII. The system can be improved further by enhancing preprocessing and with appropriate hardware selection. We are not comparing elapsed time with the Hu method because it was implemented using SAS on a different system and such a comparison would be unfair to the Hu technique.

VI. Conclusion

A novel method has been implemented for detecting the shape of a medical pill. It has increased accuracy that can be combined with the state-of-the-art color and imprint detectors together to produce a robust automatic pill identification system. This method uses the novel adaptable-ring overlay measurements to detect and classify the pill shapes. It reaches an overall accuracy of 98.7% with the Pillbox data set.

Overlay measurements produced by the adaptable ring can detect most common pill shapes and can significantly improve existing medical pill identifying applications. Moreover, this approach is both rotation and size invariant. This less computationally complex method can also be integrated with other existing VBM systems for appropriate industrial applications. It has the adaptability to add new features and define new shapes according to the application requirement.

References

[1] T. J. Moore, M. R. Cohen, and C. D. Furberg, "Serious adverse drug events reported to the Food and Drug Administration, 1998–2005," *Arch. Int. Med.*, vol. 167, pp. 1752–1759, Sep. 2007.

[2] Q. Gu, C. Dillon, and V. Burt, "Prescription drug use continues to increase: U.S. prescription drug data for 2007–2008," *NCHS Data Brief*, vol. 42, pp. 1–8, Sep. 2010.

[3] K. Frydenberg and M. Brekke, "Poor communication on patients' medication across health care levels leads to potentially harmful medication errors," *Scandin. J. Primary Health Care*, vol. 30, no. 4, pp. 234–240, 2012.

[4] D. Schneider, Y. S. Gloy, and D. Merhof, "Vision-based on-loom measurement of yarn densities in woven fabrics," *IEEE Trans. Instrum. Meas.*, vol. 64, no. 4, pp. 1063–1074, Apr. 2015.

[5] R. Anchini, G. Di Leo, C. Liguori, and A. Paolillo, "Metrological characterization of a vision-based measurement system for the online inspection of automotive rubber profile," *IEEE Trans. Instrum. Meas.*, vol. 58, no. 1, pp. 4–13, Jan. 2009.

[6] Q. Li and S. Ren, "A real-time visual inspection system for discrete surface defects of rail heads," *IEEE Trans. Instrum. Meas.*, vol. 61, no. 8, pp. 2189–2199, Aug. 2012.

[7] P. Pouladzadeh, S. Shirmohammadi, and R. Al-Maghrabi, "Measuring calorie and nutrition from food image," *IEEE Trans. Instrum. Meas.*, vol. 63, no. 8, pp. 1947–1956, Aug. 2014.

[8] S. Shirmohammadi and A. Ferrero, "Camera as the instrument: The rising trend of vision based measurement," *IEEE Instrum. Meas. Mag.*, vol. 17, no. 3, pp. 41–47, Jun. 2014.

[9] *Pillbox—Developer Resources*. accessed on Feb. 10, 2015. [Online]. Available: https://pillbox.nlm.nih.gov/developer.html

[10] Y.-B. Lee, U. Park, A. Jain, and S.-W. Lee, "Pill-ID: Matching and retrieval of drug pill images," *Pattern Recognit. Lett.*, vol. 33, no. 7, pp. 904–910, 2012.

[11] A. Hartl, C. Arth, and D. Schmalstieg, "Instant medical pill recognition on mobile phones," in *Proc. IASTED Int. Conf. Comput. Vis. (CV)*, 2011, pp. 188–195.

[12] D. Madsen *et al.*, "Automatic pill identification from pillbox images," in *Proc. Int. Conf. Comput. Vis. Theory Appl. (VISAPP)*, 2013, pp. 378–384.

[13] H. Freeman, "Computer processing of line-drawing images," *ACM Comput. Surv.*, vol. 6, no. 1, pp. 57–97, 1974.

[14] G. Loy and A. Zelinsky, "Fast radial symmetry for detecting points of interest," *IEEE Trans. Pattern Anal. Mach. Intell.*, vol. 25, no. 8, pp. 959–973, Aug. 2003.

[15] A. R. Eskandari and Z. Kouchaki, "Regular shapes detection in satellite images," *Malaysian J. Comput. Sci.*, vol. 25, no. 1, pp. 56–66, 2012.

[16] N. Barnes, G. Loy, D. Shaw, and A. Robles-Kelly, "Regular polygon detection," in *Proc. 10th IEEE Int. Conf. Comput. Vis. (ICCV)*, vol. 1. Oct. 2005, pp. 778–785.

[17] G. Loy and N. Barnes, "Fast shape-based road sign detection for a driver assistance system," in *Proc. Int. Conf. Intell. Robots Syst. (IROS)*, Sep./Oct. 2004, pp. 70–75.

[18] C. S. Nandi, B. Tudu, and C. Koley, "A machine vision-based maturity prediction system for sorting of harvested mangoes," *IEEE Trans. Instrum. Meas.*, vol. 63, no. 7, pp. 1722–1730, Jul. 2014.

[19] Y. Gan and Q. Zhao, "An effective defect inspection method for LCD using active contour model," *IEEE Trans. Instrum. Meas.*, vol. 62, no. 9, pp. 2438–2445, Sep. 2013.

[20] M.-K. Hu, "Visual pattern recognition by moment invariants," *IRE Trans. Inf. Theory*, vol. IT-8, no. 8, pp. 179–187, Feb. 1962.

[21] R. Gonzalez, R. Woods, and S. Eddins, "Representation and Description," in *Digital Image Processing Using MATLAB*, 2nd ed. Knoxville, TN, USA: Gatesmark, 2009, pp. 471–475.

[22] A. Cunha, T. Adão, and P. Trigueiros, "HelpmePills: A mobile pill recognition tool for elderly persons," *Proc. Technol.*, vol. 16, pp. 1523–1532, Dec. 2014.

[23] J. Yu, Z. Chen, and S. I. Kamata, "Pill recognition using imprint information by two-step sampling distance sets," in *Proc. 22nd Int. Conf. Pattern Recognit. (ICPR)*, Aug. 2014, pp. 3156–3161.

[24] C. Wang, S.-I. Kamata, and L. Ma, "A fast multi-view based specular removal approach for pill extraction," in *Proc. 20th IEEE Int. Conf. Image Process. (ICIP)*, Sep. 2013, pp. 4126–4130.

[25] T. Fawcett, "An introduction to ROC analysis," *Pattern Recognit. Lett.*, vol. 27, no. 8, pp. 861–874, Jun. 2006.

Kanakam Teja Maddala received the bachelor's degree in electronics and communication engineering from Jawaharlal Nehru Technological University, Kakinada, India, in 2012, and the M.S. degree in electrical engineering from the Missouri University of Science and Technology, Rolla, MO, USA, in 2015.

He has been with the Image Processing Laboratory, Department of Electrical and Computer Engineering, Missouri University of Science and Technology, since 2014. His current research interests include image processing applications, vision-based measurements, machine learning in computer vision, and medical image analysis.

Randy H. Moss (M'79–SM'92) received the B.S. and M.S. degrees in electrical engineering from the University of Arkansas, Fayetteville, AR, USA, and the Ph.D. degree in electrical engineering from the University of Illinois at Urbana–Champaign, Champaign, IL, USA.

He is currently a Professor of Electrical and Computer Engineering with the Missouri University of Science and Technology, Rolla, MO, USA, where he is also an Associate Editor of Pattern Recognition. His current research interests include primarily medical applications but also industrial applications of machine vision and image processing.

Dr. Moss was a recipient of the Society of Automotive Engineers Ralph R. Teetor Educational Award and the Society of Manufacturing Engineers Young Manufacturing Engineer Award. He was a National Science Foundation Graduate Fellow and National Merit Scholar.

William V. Stoecker received the B.S. degree in mathematics from the California Institute of Technology, Pasadena, CA, USA, in 1968, the M.S. degree in systems science from the University of California, Los Angeles, CA, USA, in 1971, and the M.D. degree from the University of Missouri, Columbia, MO, USA, in 1977.

He is currently an Adjunct Assistant Professor in computer science with the Missouri University of Science and Technology, Rolla, MO, USA, and also a Clinical Assistant Professor in dermatology with the Health Sciences Center, University of Missouri. He is currently the Editor of Computer Applications in Dermatology, McGraw-Hill, New York City, NY, USA, in 1993. He has authored or co-authored over 90 papers in dermatology, medical informatics, and related subjects. His current research interests include image analysis techniques for diagnosis of melanoma and skin cancer, medical informatics, and application of engineering methods to diagnostic problems in dermatology.

Jason R. Hagerty received the B.S. degree in computer science and computer engineering, and the M.S. degree in computer engineering from the Missouri University of Science and Technology, Rolla, MO, USA, where he is currently pursuing the Ph.D. degree in computer engineering.

He is currently with Stoecker & Associates, Rolla. His current research interests include image processing with application in the medical field and machine learning.

Justin G. Cole received the B.S. degree (Hons.) in biology from the Missouri University of Science and Technology, Rolla, MO, USA, in 2014. He is currently pursuing the M.D. degree at Indiana University, Indianapolis, IN, USA.

His current research interests include dermatology and medical informatics.

Nabin K. Mishra received the B.E. degree in electronics and communication engineering from the Institute of Engineering, Tribhuvan University, Kirtipur, Nepal, the M.S. degree in electrical engineering from Southern Illinois University Edwardsville, Edwardsville, IL, USA, and the Ph.D. degree in electrical engineering from the Missouri University of Science and Technology, Rolla, MO, USA.

He is currently involved in implementing machine learning algorithms for the data fusion of clinical and dermoscopy features for classification of melanoma involving segmentation of clinical features and artifacts in dermoscopy images. His current research interests include image processing, computer vision, classification, data mining, computational intelligence, and clustering algorithms.

R. Joe Stanley (M'99–SM'05) received the B.S.E.E. and M.S.E.E. degrees in electrical engineering and the Ph.D. degree in computer engineering and computer science from the University of Missouri, Columbia, MO, USA.

He served as an Engineering Specialist with Systems and Electronics, Inc., St. Louis, MO, USA, conducting Research and Development of imaging techniques for medical and postal applications. He is currently the Associate Chairman for Computer Engineering, Missouri University of Science and Technology, Rolla, MO, USA, where he is also an Associate Professor with the Department of Electrical and Computer Engineering. His current research interests include signal and image processing, computational intelligence, medical informatics, and automation.